Available online at www.sciencedirect.com

ScienceDirect

journal homepage: www.elsevier.com/locate/he

Hydrogen adsorption on PdGa(100), (111) and $(\bar{1}\bar{1}\bar{1})$ surfaces: A DFT study

*P. Bechthold, J.S. Ardenghi, O. Nagel, A. Juan, E.A. González, P.V. Jasen**

Departamento de Física, Universidad Nacional del Sur & IFISUR (UNS-CONICET), Av. Alem 1253, 8000 Bahía Blanca, Argentina

ARTICLE INFO

Article history:
Received 5 October 2013
Received in revised form
9 November 2013
Accepted 18 November 2013
Available online 3 January 2014

Keywords:
PdGa
DFT
Intermetallic compounds
Hydrogen adsorption

ABSTRACT

Hydrogen adsorption on PdGa intermetallic compound is analyzed using density functional theory (DFT) calculations. Changes in the electronic structure of PdGa(100), (111) and $(\bar{1}\bar{1}\bar{1})$ surfaces and H bonding after adsorption are addressed. H interacts with Pd atoms with a tilted geometry on (100) and (111) surfaces. On the $(\bar{1}\bar{1}\bar{1})$ surface two possible forms for H adsorption are detected: one is observed atop perpendicular to the surface and the other one is subsuperficial, both with similar adsorption energies. The Ga–H interaction is energetically less stable and is only present on the (100) plane. Pd–Pd bond strength decreases up to 53.8% as the new Pd–H bond is formed. The Pd–H bond length differs less than 1%, compared to the gas phase value for the (100), (111) and atop $(\bar{1}\bar{1}\bar{1})$. However in the $(\bar{1}\bar{1}\bar{1})$ subsurface-H bond length is about 2.17 Å. The effect of H is limited to its first Pd neighbor. Analysis of orbital interaction reveals that the Pd–H bond mainly involves s–s and s–p orbitals with lower participation of Pd 4d orbitals. The computed H vibration frequencies after adsorption show values of 1786, 1289 and 633.5 cm^{-1} that correspond to top, bridge and hollow sites respectively.

1. Introduction

In the last few years, intermetallic compounds (IMC) formed by transition metals (TM) and main group metals has attracted much attention as efficient and highly selective catalysts. It has been argued that the isolation and regular distribution of the active sites on their surfaces play a very important role [1].

The IMC PdGa is an interesting system that has been experimentally and theoretically studied in recent years [1–18]. This IMC has been mainly analyzed as a catalyst in the selective hydrogenation of acetylene [2–4]. Typical catalysts utilized in these reactions are made of Pd dispersed on metal oxides, and has the drawback of frequently deactivation under hydrogenation conditions by the formation of a carbonaceous deposit resulting from the polycondensation of unsaturated compounds [3]. Adding promoters or alloying Pd with other metals has result in an increased selectivity and long-term stability in the hydrogenation of acetylene [5]. The size of active sites must be restricted preventing the formation of ensembles of Pd on the surface – so-called active-site isolation- and increasing catalyst selectivity [7]. The formation

* *Corresponding author*. Tel.: +54 291 4595101x2843; fax: +54 0291 4595142.
E-mail address: pjasen@uns.edu.ar (P.V. Jasen).

0360-3199/$ – see front matter
http://dx.doi.org/10.1016/j.ijhydene.2013.11.077

of palladium hydrides influences the selectivity. Also the depletion of subsurface hydrogen and/or a lower barrier for C_2H_{2+x} intermediate desorption modify the selectivity of Pd-based catalyst [6]. Armbrüster et al. reported that the IMC PdGa is a highly active, selective and stable catalyst for the semi-hydrogenation of acetylene in a large excess of ethylene [8]. Armbrüster et al. also described a strong covalent bond between Pd and Ga atoms providing long-term stability for the catalysts under reaction conditions [9].

On the other hand, steam reformation of methanol (MSR, $CH_3OH + H_2O \rightarrow CO_2 + 3H_2$) is an active process for supplying hydrogen in a down-stream proton-exchange membrane fuel cells (PEMFCs). CO formation has to be avoided because it poisons the anode at the fuel cell. There are several papers related to MSR, among them many use Pd–Ag as a catalyst. The production of H_2 at low-pressure MSR using PdAg membrane reactor was studied by Ghasemzadeh et al. [19] and Iulianelli et al. [20]. The effect of oxygen in a flat Pd–Ag reactor was published by Basile et al. [21]. Gallucci & Basile compared the performance of a Pd–Ag reactor using different fuels [22]. The MSR over Ni supported on Ni–Sn nano particles was recently published by Bobadilla et al. [23]. Friedrich et al. presented a study on ZnPd/ZnO systems with high CO_2 selectivity in MSR [24].

Recently, Fottinger studied the effect of CO on intermetallic PdZn/ZnO and Pd_2Ga/Ga_2O_3 MSR catalyst [25]. This author found a strong Pd–CO interaction leading to an enrichment of Pd at the surface and limiting catalysts stability.

Rameshan et al. performed XPS studies *in situ* for MSR on PdGa and concluded that O_2 addition improves catalytic selectivity to CO_2 [26].

Although, the use of bare IMC PdGa is promising for both acetylene hydrogenation and MSR catalyst the fundamentals of hydrogen interaction in the surfaces exposed is not fully understood yet. DFT calculations provide an additional means to interpret and predict the H-adsorption behavior of these materials.

Koc et al. [12] investigated the structural, elastic, electronic, optical, and vibrational properties of a cubic PdGa compound using the norm-conserving pseudopotentials within the local density approximation (LDA). These authors found that the cubic PdGa compound is in the ground-state configuration and that the band structures are metallic in nature. Calculated phonon dispersion curves have no soft modes at any vectors, thus confirming the stability of PdGa.

While the surfaces of simple close-packed transition metals (TM) have only a few non-equivalent reaction sites, the surfaces of complex TM intermetallics provide a rich variety of different adsorption sites, leading to a several of possible reaction channels for catalytic reactions. The main motivation behind the intermetallic compound concept is to obtain long-term stable catalysts with pre-selected electronic and local structural properties [1].

Prinz et al. determined and explored the stable surface terminations of PdGa [14]. The authors combine quantitative low-energy electron diffraction (LEED), high-resolution scanning tunneling microscopy (STM) and ab initio thermodynamics calculations to unequivocally identify the surface terminations of PdGa(111) and PdGa($\bar{1}\bar{1}\bar{1}$) surfaces with vacancies. These surfaces shown significant differences in catalytic activity for hydrogen dissociation. These authors have determined that IMC PdGa:B(111)Pd_3 and PdGa:B($\bar{1}\bar{1}\bar{1}$) Pd_1 are the more stable surface terminations. Structural differences of both surface terminations lead to significant energetic differences in the catalytic dissociation of a molecular hydrogen. Moreover, the structural dissimilarity of (111) and ($\bar{1}\bar{1}\bar{1}$) surfaces turns IMC PdGa into a prototype model system [14].

Krajčí and Hafner investigated the {111} threefold surfaces polar character of the PdGa compound using DFT methods [13]. Due to the lack of inversion symmetry, the B20 structure exists in two enantiomorphic forms denoted as A and B, as in [15,16]. In both non-equivalent (111) and ($\bar{1}\bar{1}\bar{1}$) directions the formation of several surfaces differing in structure and chemical composition are possible. Eight possible surface terminations with different atomic layers in surface and sub-surface positions were identified. Calculated surface energies are in agreement with a simulated cleavage experiment. However, cleavage does not result in the formation of the lowest-energy surfaces, because all possible {111}-cleavage planes expose a low-energy surface on one side, and a high-energy surface on the other side. The calculated surface density of states is in very good agreement with photoemission spectroscopy experiments and calculated STM images of the most stable surfaces are in agreement with all the details of experimental images available [13].

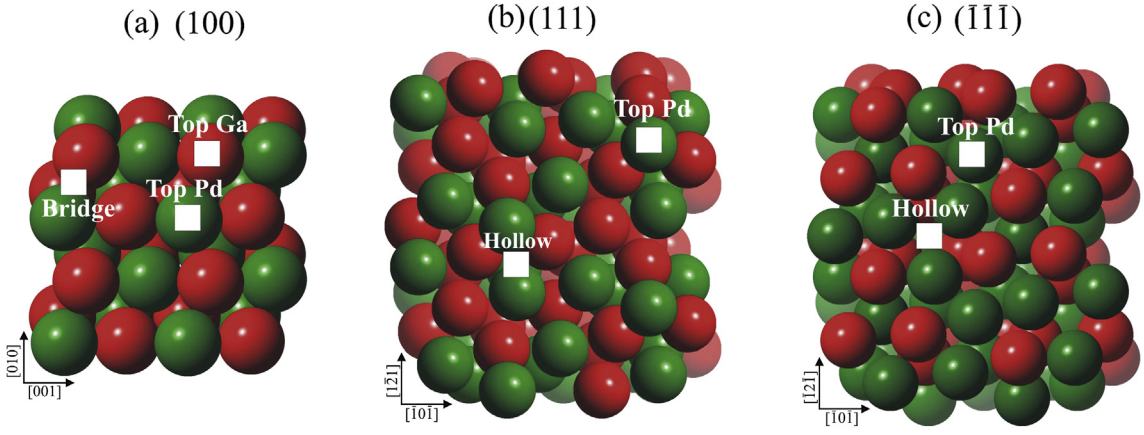

Fig. 1 – Schematic top view of PdGa: (100) (a), (111) (b) and ($\bar{1}\bar{1}\bar{1}$) (c) surfaces. The adsorption sites are indicated. ● Pd, ● Ga.

The purpose of the present work is to compare our previous theoretical study on the PdGa intermetallic compound [4,10], considering other possible planes that can be exposed at the real catalyst surface. DFT calculations are performed in order to determine binding energies of one hydrogen atom on the IMC PdGa (100), (111) and $(\bar{1}\bar{1}\bar{1})$ surfaces. Changes in the electronic structure and bonding of PdGa surfaces as well as changes in the surface bonding are also analyzed after H adsorption.

2. Surface models and computational method

The PdGa IMC presents a $P2_13$ structure with a lattice parameter of $a_0 = 4.909$ Å [16,27–29]. The Bravais lattice is simple cubic, but the overall point symmetry is tetrahedral. In this structure, seven Ga atoms surround each Pd. A refined crystal structure of (1:1) PdGa was recently reported [16]. In order to continue with this study on the intermetallic compound, we selected the low-index surfaces {100} and {111} for a better understanding of their adsorption capabilities. The reasons for selecting these surfaces are a comparison them with our previous calculations in the (110) surface and because in the close packed cubic crystal they present a higher stability. The PdGa (100) surface is stoichometric and uniquely defined, while the polarity along the <111> directions make (111) and $(\bar{1}\bar{1}\bar{1})$ surfaces non-equivalent. These two surfaces also have two enantiomorphic forms. Form A is defined by the atomic positions of Ga (x = y = z = 0.84284) and Pd (x = y = z = 0.14234). On the other hand, the enantiomorphic form B is defined by inversion. Considering the polarity and the two enantiomorphs, we have 16 possible (1x1) terminations for surfaces along the [111] and $(\bar{1}\bar{1}\bar{1})$ directions. We have selected the form B and studied the Pd_1 termination using the notation presented by Roshental et al. [15]. The reason for this selections is because, according to Prinz et al., experimental and theoretical STM simulation indicated that

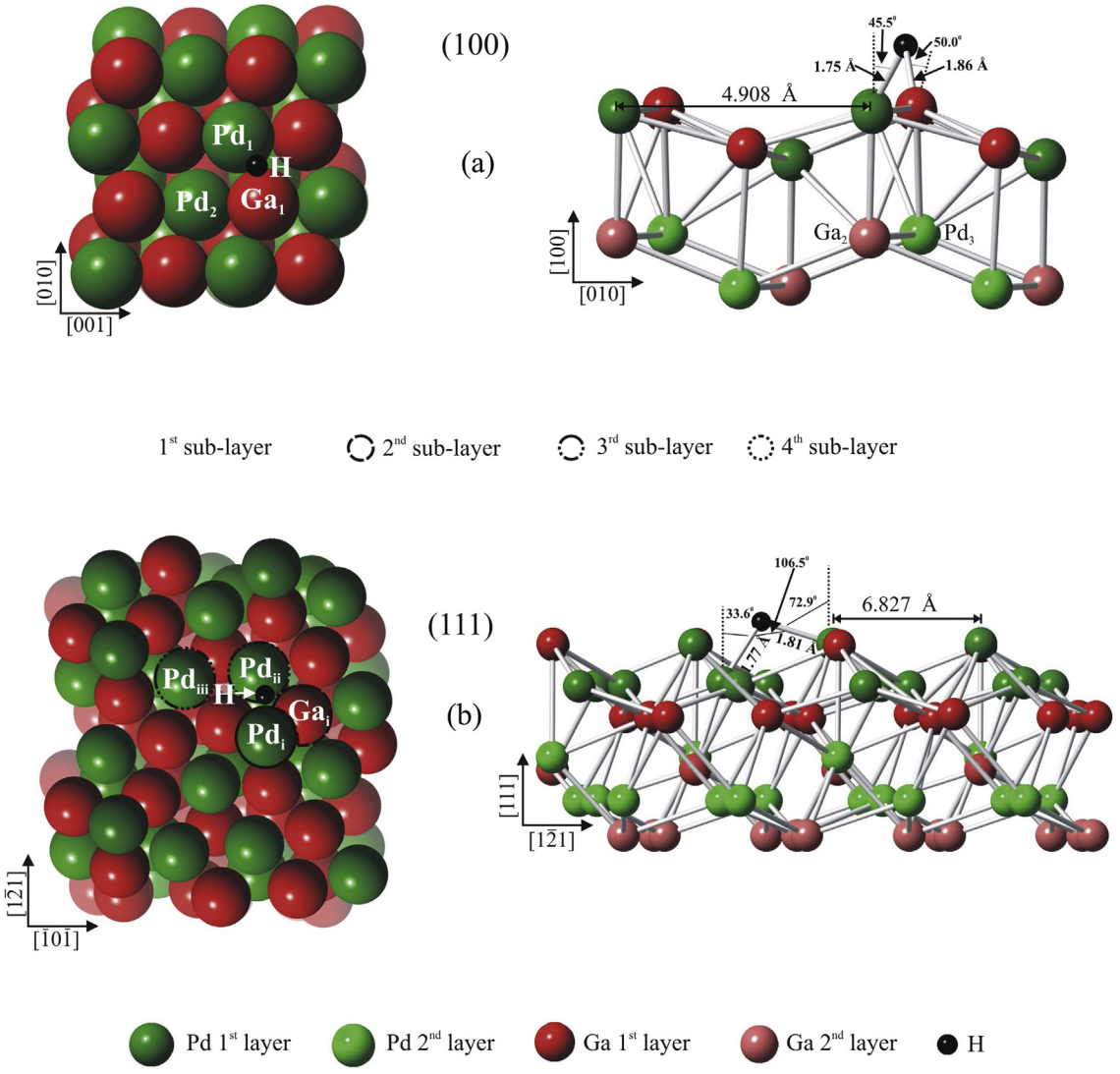

Fig. 2 – Schematic top (right) and lateral (left) view of PdGa: (100) (a) and (111) (b) surfaces after H adsorption in the more stable geometry. For sake of clarity, only two first layers are shown.

PdGa:B(111)Pd_3 and PdGa:B($\bar{1}\bar{1}\bar{1}$) Pd_1 are the actual surfaces structure [14]. In the case of PdGaB(111) we studied the Pd_1 terminated structure in order to make a better comparison with the PdGa:B($\bar{1}\bar{1}\bar{1}$) Pd_1 structure because we are interested in the Pd isolated site concept.

2.1. *Computational method*

We performed first-principles calculations based on spin polarized DFT. The Vienna *Ab-initio* Simulation Package (VASP) is used to solve Kohn–Sham equations with periodic boundary conditions and a plane wave basis set [30–32]. Electron–ion interactions were described by ultra-soft pseudopotentials [33]; exchange and correlation energies were also calculated using the Perdew–Burke–Ernzerhof form of the spin-polarized generalized gradient approximation (GGA-PBE) [34]. We used a kinetic energy cutoff of 700 eV for all calculations, which converges total energy to ~1 meV/atom and 0.001 Å for the primitive bulk cell. The Monkhorst–Pack scheme is used for k-point sampling [35]. An equilibrium lattice constant of 4.899 Å is used as obtained with a 7 × 7 × 7 converged mesh within the first Brillouin Zone. Geometry optimization was terminated when the Hellman–Feyman force on each atom was less than 0.02 ev/Å and the energy difference was lower than 10^{-6} eV. The computed lattice constant is in agreement with experimental XRD data (4.89695 Å) [16]. Bader analysis is used to calculate electron charges on atoms before and after H adsorption [36].

We defined the cohesion energy H/PdGa with respect to isolated atoms by:

$$\Delta E_{\text{cohesion}} = E_{\text{Total}}(H/PdGa) - E_{\text{Total}}(PdGa) - E_{\text{Total}}(H_{\text{atom}}) \quad (1)$$

The stabilization of H/PdGa can be further investigated by comparing the adsorption energies of H/PdGa -starting from the intermetallic surface and molecular hydrogen- given by:

$$\Delta E_{\text{adsorption}} = E_{\text{Total}}(H/PdGa) - E_{\text{Total}}(PdGa) - \frac{1}{2}E_{\text{Total}}(H_2) \quad (2)$$

In both expressions the first term on the right-hand side is the total energy of the super cell that includes 32 Pd and 32 Ga atoms for the (100); or 84 Pd and 84 Ga atoms for (111) and

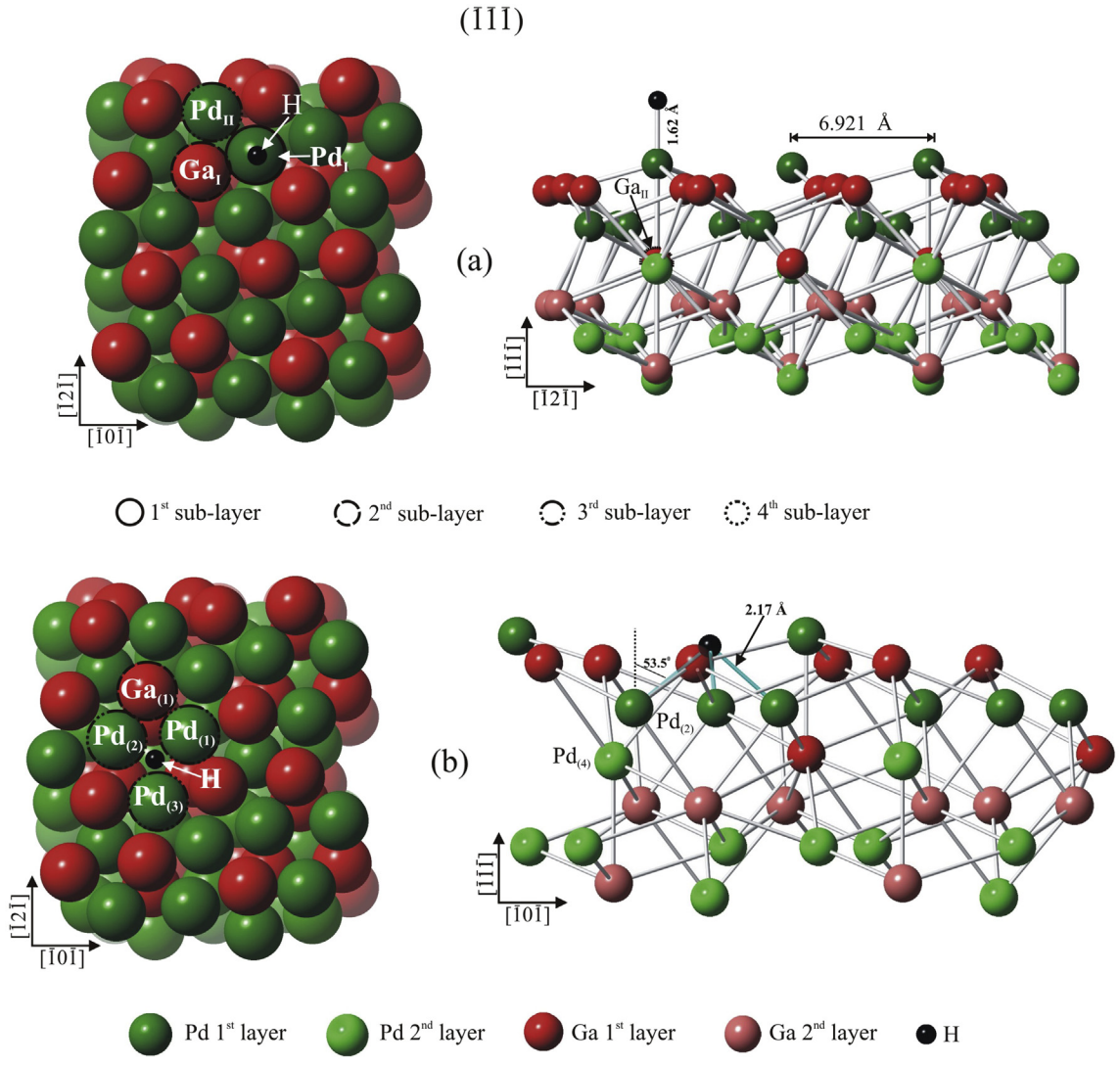

Fig. 3 – Schematic top (right) and lateral (left) view of PdGa($\bar{1}\bar{1}\bar{1}$) surface after H adsorption in the more stable geometry. For sake of clarity, only two first layers are shown.

$(\bar{1}\bar{1}\bar{1})$ plus one hydrogen atom; the second term represents the total energy of the bare intermetallic super cell. Meanwhile, the third term is the energy of one isolated H atom or the half hydrogen molecule total energy. The energy of isolated H or H_2 was determined from calculations performed on single species in a cubic cell with 10 Å sides and carrying out a Γ-point calculation. We obtained a H_2 bond length of 0.751 Å and a binding energy of −4.52 eV. These values are in agreement with experimental data (0.741 Å, −4.75 eV) [37].

In order to understand H–PdGa interactions and bonding, we used the concept of Density of States (DOS) and the Crystal Orbital Overlap Population (COOP) as described by Hoffmann [38]. The COOP curve is a plot of the overlap population (OP) weighted DOS vs. energy. Looking at the COOP, we analyzed the extent to which specific states contribute to a bond between atoms or orbitals. The SIESTA code was used to compute COOPs and OPs [39,40].

2.2. *Surfaces and adsorption model*

We represented the (100), (111) and $(\bar{1}\bar{1}\bar{1})$ planes with supercells. In order to achieve the best compromise between computational time and accuracy in our model, we decided to use a seven-layer slab separated in the corresponding perpendicular-direction by vacuum regions. It should be pointed out that each "layer" is formed by two "sub-layers", presenting atoms above and below for the (100) surface (see Fig. 1a); and four "sub-layers" for the (111) and $(\bar{1}\bar{1}\bar{1})$ surfaces (see Fig. 1b and c). We also tested our calculations with 9 and 11 layers (and their corresponding sub layers) and no further improvement in energy was found. The thickness of the vacuum region, corresponding to 14 Å, was enough in order to avoid the interaction of H with the other surfaces. The chosen thickness of the PdGa surfaces slab approximates the electronic structure of 3D bulk PdGa in the innermost layer. As we mentioned before for the (111) and $(\bar{1}\bar{1}\bar{1})$ planes, we have used the form B and Pd_1 termination.

For the study of H adsorption on the PdGa surfaces at low coverage, the H-surface distance was optimized considering relaxation for the first four layers of the slab until 1 meV convergence was obtained in the total energy, while maintaining the three remaining layers fixed. Due to the Pd coordination in the bulk structure, almost any exposed plane presented isolated Pd sites, being the next Pd neighbor located at a distance of 4 Å or more (except in the (100) plane). Fig. 2 shows a schematic top (right) and side (left) view of the surfaces after H adsorption, for (100) and (111) surfaces respectively, while Fig. 3 shows the $(\bar{1}\bar{1}\bar{1})$ surface.

3. Results and discussion

The results for bulk PdGa were presented in a previous paper [4]. Recent calculations from Krajčí and Hafner [13] and Koc et al. [12] for the same PdGa crystal structure are in agreement with our theoretical results.

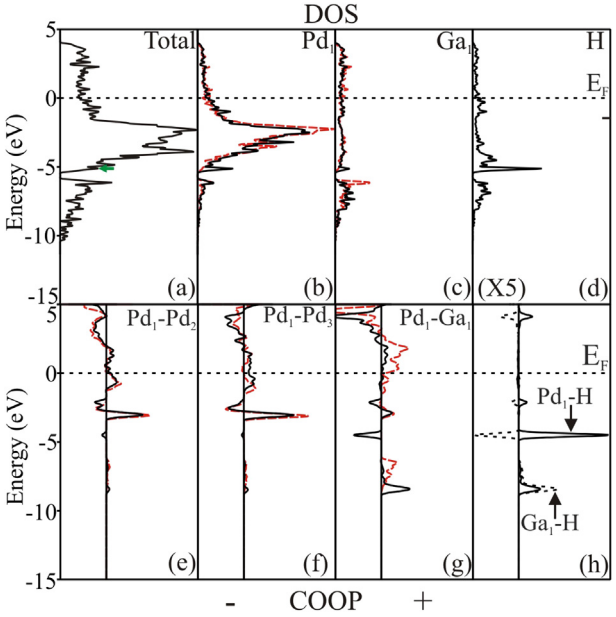

Fig. 4 – Total DOS curves for PdGa(100) + H (a), projected DOS for a Pd_1 atom (b), projected DOS for a Ga_1 atom (c) and projected DOS for an H atom (d). COOP curves for Pd–Pd (e)–(f), Pd–Ga (g), Pd–H and Ga–H (h) bonds before (red dashed line) and after (black filled line) H adsorption. The green arrow in (a) indicates the interaction with H. The bar on the right in figure (d) represents the H 1s state before adsorption. (For interpretation of the references to color in this figure legend, the reader is referred to the web version of this article.)

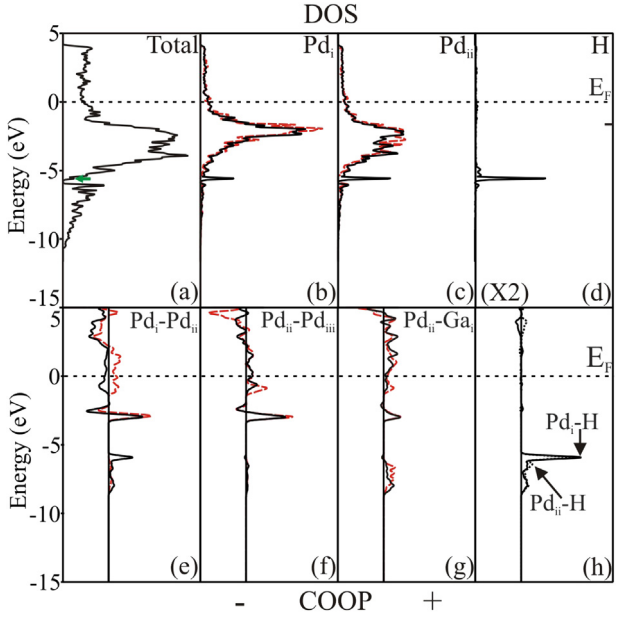

Fig. 5 – Total DOS curves for PdGa(111) + H (a), projected DOS for a Pd_i atom (b), projected DOS for a Pd_{ii} atom (c) and projected DOS for an H atom (d). COOP curves for Pd–Pd (e)–(f), Pd–Ga (g), Pd–H (h) bonds before (red dashed line) and after (black filled line) H adsorption. The green arrow in (a) indicates the interaction with H. The bar on the right in figure (d) represents the H 1s state before adsorption. (For interpretation of the references to color in this figure legend, the reader is referred to the web version of this article.)

Considering the surface of the slab, after relaxation, the interlayer spacing in our models changes less than 1% from the first layer to the inner ones. The distances between two adjacent Pd top sites on the surface are 4.908 Å, 6.827 Å and 6.921 Å in the (100), (111) and $(\bar{1}\bar{1}\bar{1})$ planes and the mean Pd–Ga distances are 2.610 Å, 2.550 Å and 2.501 Å, respectively.

The bulk solid electronic structure was previously discussed in [4]. The PdGa also presents a significantly reduced electron density at the Fermi level (see Figs. 4–7a–d). The Total DOS for the three surfaces considered look similar; however, differences can be appreciated in the surface atoms projections. The Total DOS of (111) and $(\bar{1}\bar{1}\bar{1})$ surfaces are similar to that reported by Prinz et al. [14, supporting information]. The Pd projected DOS for the planes (111) and (100) is similar to the one already published for the plane (110) [4] and shows a broad Pd 4d dominated band with a peak at about −2.9 eV in good agreement with the recent calculations made by Krajčí and Hafner [13]. In the case of $(\bar{1}\bar{1}\bar{1})$ plane, the Pd d projection is narrowed and similar to the Pd projection in GM (Ga_1 surface termination according to Rosenthal notation [15]) case in Ref. [13]. In all cases, Ga projected DOS is represented by s- and p-like states, being the Ga in the (111) plane ($s^{1.86}$ $p^{0.50}$) the most populated.

Regarding the bonding, the OP values for Pd–Pd and Pd–Ga are presented in Table 1. The Pd–Pd OP in the (100) and (111) surfaces is about 0.106–0.119 at distances ranging from 2.875 to 3.011 Å. These values are higher than the ones obtained for Pd–Pd bulk (0.090). In the case of the $(\bar{1}\bar{1}\bar{1})$ surface, the Pd–Pd OP is close to the bulk value at a shorter bond distance (2.948 Å). In our previous study, we obtained a Pd–Pd OP of 0.146 for the (110) surface [4]. The Pd–Ga OP are higher than those of the bulk value in the (111) and $(\bar{1}\bar{1}\bar{1})$ surfaces (42.3% and 56.2%, respectively) at shorter distances (−9.5% and −4.4% from the bulk solid, respectively). However, in the (100) surface the Pd–Ga OP are lower than bulk values at distances of 2.607 and 2.643 Å.

Orbital by orbital contributions to the OP between atoms in the PdGa surfaces are summarized in Table 2. The main interactions are s–s and s–p followed by p–d and p–p. The s–s and s–p contributions are higher and lower respectively for the Pd–Pd bond in the (111) plane compared to the other surfaces. This is in line with a higher (lower) Pd s (p) population. The bonding scheme presents higher s–p and p–d contributions when compared to the (110) surface [4]. No d–d interaction is detected. Considering the Pd–Ga bond, the scheme is similar to the one reported for the (110) surface [4] being the s–p contribution higher than 65% while a p–d contribution is close to 18%.

3.1. *Hydrogen adsorption on the relaxed PdGa surfaces at low coverage*

We found different H-adsorption geometries in the three considered surfaces. While in the (100) and (111) surfaces the H's are tilted, in the $(\bar{1}\bar{1}\bar{1})$ the adsorption is perpendicular to the

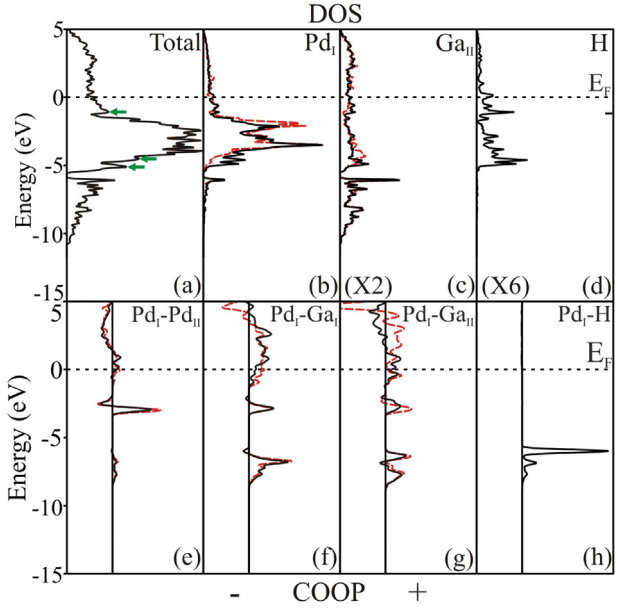

Fig. 6 – Total DOS curves for PdGa($\bar{1}\bar{1}\bar{1}$) + H on atop geometry (a), projected DOS for a Pd_I atom (b), projected DOS for a Ga_{II} atom (c), and projected DOS for an H atom. COOP curves for Pd–Pd (e), Pd–Ga (f)-(g), Pd–H (h) bonds before (red dashed line) and after (black filled line) H adsorption. The green arrow in (a) indicates the interaction with H. The bar on the right in figure (d) represents the H 1s state before adsorption. (For interpretation of the references to color in this figure legend, the reader is referred to the web version of this article.)

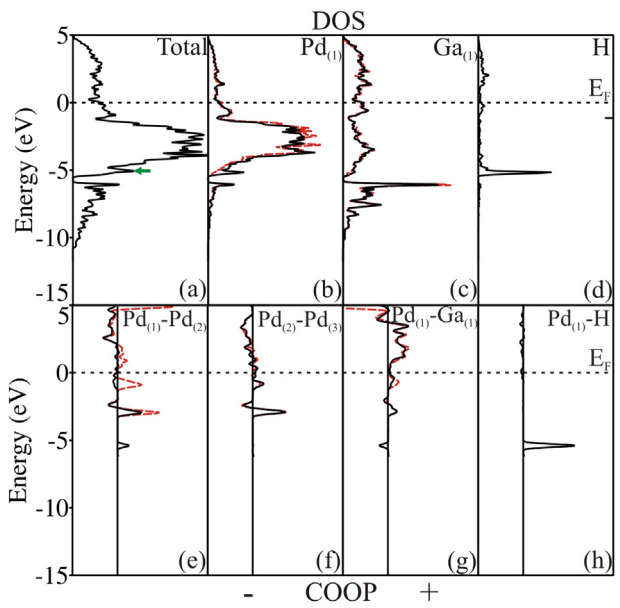

Fig. 7 – Total DOS curves for PdGa($\bar{1}\bar{1}\bar{1}$) + H in a hollow geometry (a), projected DOS for a $Pd_{(1)}$ atom (b), projected DOS for a $Ga_{(1)}$ atom (c), and projected DOS for an H atom. COOP curves for Pd–Pd (e–f), Pd–Ga (g), Pd–H (h) bonds before (red dashed line) and after (black filled line) H adsorption. The green arrow in (a) indicates the interaction with H. The bar on the right in figure (d) represents the H 1s state before adsorption. (For interpretation of the references to color in this figure legend, the reader is referred to the web version of this article.)

Table 1 – Electron orbital occupation, overlap population (OP), ΔOP% and distances for PdGa low-index planes before and after H adsorption.

Structure	Electronic occupation			Bond	OP	ΔOP%[a]	Distances (Å)
	s	p	d	Type			
PdGa(100)							
Pd	0.74	0.32	9.80	Pd_1–Pd_2	0.106		3.011
				Pd_1–Pd_3	0.118		2.875
Ga	1.73	0.42	0.00	Pd_1–Ga_1	0.116		2.643
				Pd_1–Ga_2	0.124		2.607
PdGa(100) + H (bridge)							
Pd	0.62	0.54	9.77	Pd_1–Pd_2	0.067	−36.8	3.070
				Pd_1–Pd_3	0.091	−22.9	2.960
Ga	1.69	0.47	0.00	Pd_1–Ga_1	0.025	−78.5	2.614
				Pd_1–Ga_2	0.111	−10.5	2.686
H	1.41	0.00	0.00	Pd_1–H	0.516		1.749
				Ga_1–H	0.111		1.856
PdGa(111)							
Pd	0.91	0.24	9.83	Pd_i–Pd_{ii}	0.106		3.007
				Pd_{ii}–Pd_{iii}	0.119		2.994
Ga	1.86	0.50	0.00	Pd_i–Ga_i	0.195		2.487
				Pd_{ii}–Ga_i	0.125		2.591
PdGa(111) + H (hollow)							
Pd	0.61	0.38	9.80	Pd_i–Pd_{ii}	0.049	−53.8	2.849
				Pd_{ii}–Pd_{iii}	0.086	−27.7	3.021
Ga	1.66	0.45	0.00	Pd_i–Ga_i	0.153	−21.5	2.610
				Pd_{ii}–Ga_i	0.086	−31.2	2.500
H	1.37	0.00	0.00	Pd_i–H	0.358		1.807
				Pd_{ii}–H	0.362		1.769
PdGa($\bar{1}\bar{1}\bar{1}$)							
Pd	0.65	0.36	9.77	Pd_I–Pd_{II}	0.088		2.948
Ga	1.68	0.43	0.00	Pd_I–Ga_I	0.195		2.451
				Pd_I–Ga_{II}	0.214		2.488
PdGa($\bar{1}\bar{1}\bar{1}$) + H (top)							
Pd	0.54	0.61	9.70	Pd_I–Pd_{II}	0.062	−29.5	3.017
Ga	1.69	0.40	0.00	Pd_I–Ga_I	0.155	−20.5	2.530
				Pd_I–Ga_{II}	0.184	−14.1	2.467
H	1.47	0.00	0.00	Pd_I–H	0.644		1.616
PdGa($\bar{1}\bar{1}\bar{1}$)							
Pd	0.70	0.38	9.77	$Pd_{(1)}$–$Pd_{(2)}$	0.106		3.021
				$Pd_{(2)}$–$Pd_{(4)}$	0.061		3.080
Ga	1.71	0.40	0.00	$Pd_{(1)}$–$Ga_{(1)}$	0.105		2.670
PdGa($\bar{1}\bar{1}\bar{1}$) + H (hollow)							
Pd	0.55	0.40	9.75	$Pd_{(1)}$–$Pd_{(2)}$	0.038	−64.1	3.022
				$Pd_{(2)}$–$Pd_{(4)}$	0.077	+26.0	3.079
Ga	1.72	0.36	0.00	$Pd_{(1)}$–$Ga_{(1)}$	0.077	−26.7	2.673
H	1.47	0.00	0.00	$Pd_{(1)}$–H	0.190		2.169
				$Pd_{(2)}$–H	0.189		2.169
				$Pd_{(3)}$–H	0.185		2.172

[a] The corresponding clean surface is used as a reference to compute ΔOP%.

surface interacting with only one Pd atom (see Figs. 2 and 3a), in addition the ($\bar{1}\bar{1}\bar{1}$) presents a subsurface site for H location (see Fig. 3b). The adsorption and cohesion energy stabilization order is (111)-hollow > (100)-bridge > ($\bar{1}\bar{1}\bar{1}$)-top (see Table 3). The Pd–H bond lengths are 1.769 and 1.807 Å for (111), 1.749 Å for (100) and 1.616 Å for respectively. The Pd–H distances are higher than the DFT computed for the molecular species in the gas phase (1.541 Å) [41]. The Pd–H bond length in the ($\bar{1}\bar{1}\bar{1}$) surface is close to the one reported for the top-adsorption on the (110) surface (1.621 Å), with a similar H-adsorption energy. In all cases considered, the stabilization energy is higher than that in the (110) plane [4]. Our computed stabilization value for the (111) surface (−1.18 eV) is very close to the one recently reported by Prinz et al. [14, supporting information]. The best configuration reported by these authors is a hollow site on the surface Pd_3 trimmer (−1.13 eV per H pair). We have also detected the H–Pd trimmer interaction in a subsurface location because the surface cut is performed one sublayer below to the one used by Prinz et al. [14, supporting information].

Our prediction of the site geometry can also be compared to calculations on metallic FCC Pd surfaces. Tománek et al. found a three-fold site as the most stable one on the (110) unreconstructed surface with a computed Pd–H distance of 1.8 Å [42]. Ledentu et al. reported an energy of 0.469 eV/H and a Pd–H distance of 1.79–1.82 Å at 1.5 ML coverage [43]. Dong et al. reported a systematic DFT study of the reconstruction on Pd(110);

Table 2 – Orbital by orbital percentage contributions to Pd–Pd, Pd-Ga, Pd–H, and Ga–H overlap populations (% COOP) for H/PdGa(100), (111) and $(\bar{1}\bar{1}\bar{1})$ system.[a]

	PdGa (100)					
	Pd_1–Pd_2		Pd_1–Ga_1		Pd_1–H	Ga_1–H
	Clean	H	Clean	H	H	H
s–s	26.2	20.0	4.3	0.0	51.0	0.0
s–p	40.2	37.3	69.7	45.5	47.2	100.0
s–d	6.7	6.8	0.0	1.5	1.8	–
p–p	10.1	16.3	8.1	26.6	–	–
p–d	16.8	19.6	17.9	26.4	–	–
d–d	0.0	0.0	–	–	–	–
	PdGa (111)					
	Pd_i–Pd_{ii}		Pd_{ii}–Ga_i		Pd_i–H	Pd_{ii}–H
	Clean	H	Clean	H	H	H
s–s	32.6	0.0	7.5	2.3	56.0	56.2
s–p	35.3	47.0	65.5	63.6	41.5	40.7
s–d	4.3	8.6	0.4	0.0	2.5	3.1
p–p	8.5	17.9	9.0	8.8	–	–
p–d	18.9	26.3	17.6	25.3	–	–
d–d	0.0	0.2	–	–	–	–
	PdGa $(\bar{1}\bar{1}\bar{1})$ top					
	Pd_I–Pd_{II}		Pd_I–Ga_{II}		Pd_I–H	–
	Clean	H	Clean	H	H	–
s–s	18.9	6.9	11.6	22.9	52.7	–
s–p	38.7	30.4	67.9	40.6	45.2	–
s–d	7.8	10.0	0.0	0.0	2.1	–
p–p	10.2	23.8	1.8	19.0	–	–
p–d	24.4	28.9	18.7	17.5	–	–
d–d	0.0	0.0	–	–	–	–
	PdGa $(\bar{1}\bar{1}\bar{1})$ hollow					
	$Pd_{(1)}$–$Pd_{(2)}$		$Pd_{(1)}$–$Ga_{(1)}$		$Pd_{(1)}$–H	–
	Clean	H	Clean	H	H	–
s–s	26.6	0.0	8.9	8.2	47.3	–
s–p	37.9	26.4	60.1	54.3	51.2	–
s–d	6.0	11.7	0.0	0.0	1.5	–
p–p	12.2	28.5	13.2	13.7	–	–
p–d	17.3	33.4	17.8	23.8	–	–
d–d	0.0	0.0	–	–	–	–

[a] See Figs. 4 and 5.

the adsorption energy and geometry in a (2 × 1) H/Pd(110) at 1 ML is 0.494 eV/atom and the Pd–H distance is 1.81 Å [44]. Ahmed et al. simulated the dissociative adsorption of H_2 on Pd(111) and showed that a three fold FCC hollow site was stable with Pd–H distances ranging from 1.78 to 1.81 Å [45]. Gladys et al. computed a minimum energy of 0.489 eV at a four fold hollow in Pd(100) with a Pd–H vertical distance of 0.45 Å [46].

Regarding the H adsorption on Ga sites we found only one favorable site. This adsorption presents a top geometry that is less stable than any Pd sites and is only present on the (100) surface. There is also another possible Ga–H interaction on the same surface. The most stable corresponds to the adsorption on a Pd–Ga bridge site (see Pd_1–H and Ga_1–H in Fig. 2a) with an Ga–H distance of 1.856 Å. This value is close to the one reported by Himmel et al. in Ga_2H_2 (1.8729 Å) [47].

Considering the electronic structure, the total DOS is dominated by the many bulk-like and surface Pd and Ga atoms. When bonding to the surface, an electron transfer from Pd atoms to H atom occurs (Ga atoms practically do not participate) to the extent of 0.37–0.40e^-. Figs. 4–7 shows the total DOS of the system with H contributions. The bar on the right in the DOS plots indicates the energy level of the H 1s orbital with respect to the E_F before interaction. After adsorption, this level is stabilized in all surfaces sites considered. We also found that after H adsorption, the d band is modified in all cases. In general, the electron density decreases, some peaks are missing and a peak at −5.2 and −5.7 eV is developed in the (100) and (111) surfaces respectively (see Figs. 4a and 5a). Prinz et al. reported an H projection with a peak at −5.7 eV in the (111) surface. In the case of the $(\bar{1}\bar{1}\bar{1})$ surface, three peaks are developed between −5.7 eV and E_F (see Fig. 6a) [14].

The H projection also reveals some weak interaction with Ga in the (100) bridge adsorption site (see Fig. 4c, d and f). This interaction is not present in the (111) and $(\bar{1}\,\bar{1}1)$ surfaces.

The projected DOS of Pd_i and Pd_{ii} reveals an interaction with H in the (111) surface. Both Pd atoms present a peak at −5.7 eV, at the same energy values where a sharp peak where the H projection is located (compare Fig. 5b and c with Fig. 5d). In the case of the $(\bar{1}\bar{1}\bar{1})$ surface, H projection presents a bandwidth of about 5.5 eV (see Fig. 6d) that interacts mainly with the Pd d band. Prinz et al. reported a similar computed H-projection on the (111) surface for a Pd_3 trimmer surface site

Table 3 – Adsorption, Cohesion energies, vibrational frequencies, Pd–H bond length and tilt angle for PdGa surfaces after H adsorption.[a]

Surfaces	(100)			(111)		$(\bar{1}\bar{1}1)$	
Adsorption site	Top Pd	Top Ga	Bridge	Top	Hollow	Top	Hollow
E_{ads} (eV/H)	−0.70	−0.50	−0.95	−0.30	−1.18	−0.65	−0.67
E_{coh} (eV/H)	−1.85	−1.65	−2.11	−1.45	−2.33	−1.80	−1.82
ν (cm^{-1})	–	–	1289.9	–	1206.2	1786.1	633.5
Pd–H (Å)	1.700	1.600[b]	1.749	1.700	1.807	1.616	2.172
					1.769		2.169
							2.169
Tilt angle (°)	–	–	45.5	–	72.9	0.06	53.5
					33.6		

[a] The geometries for the minimal configuration are shown in Figs. 2 and 3.
[b] In this case we report Ga–H bond distances.

bonded to H at −6.2 eV [14, supporting information]. We also found a favorable hydrogen adsorption in a hollow site on the $(\bar{1}\bar{1}\bar{1})$ surface. The adsorption energy in this site is close to the top configuration (−0.67 vs −0.65 eV). In this case, the H is interacting with three Pd atoms, $Pd_{(1)}$, $Pd_{(2)}$ and Pd $_{(3)}$ (see Fig. 3b, representing a subsurface H). The Pd–H bond length is the longest among all PdGa surfaces considered (2.169 Å). The H projected DOS also presents a sharp peak at −5 eV and no interaction with Ga is detected.

Analysis of the bonding between H and the surface in Table 2 reveals that the main contribution to the Pd–H bond in all surfaces considered comes mainly from H 1s-Pd 5s and 5p orbitals and less than a 2.5% from d orbitals. In the case of Ga–H (only on the (100) surface) the main contribution is H 1s − Ga 4p. In addition, Table 2, shows that the s–s and s–p contributions to the Pd–Pd or Pd–Ga bonding decrease while p–p and p–d contributions increase. As mentioned before, s and p orbitals are participating in the Pd–H (Ga–H) bond.

As shown in Table 1, the Pd–H (and Ga–H) bond is achieved at the expense of weakening Pd–Pd nearest neighbors in Figs. 2 and 3. Thus, the Pd_1–Pd_2 (Fig. 2a), Pd_i–Pd_{ii} and Pd_{ii}–Pd_{iii} (Fig. 2b) and Pd_I–Pd_{II} (Fig. 3a) directly bonded to H have reduced their OP between 29.5 and 53.8% of their original values on the clean surface. The Pd–Ga OP is also reduced being the Pd_1–Ga_1 on (100) the most affected (78%). It is interesting to mention that the Pd–H bond developed in a subsurface hollow site on the $(\bar{1}\bar{1}\bar{1})$ surface is also achieved at the expenses of the Pd–Pd bonds, and that three new Pd–H bonds are formed. This configuration presents the highest decrease in Pd–Pd OP (64.1%).

COOP curves in Figs. 4–7 allow us to interpret which bonding or antibonding states changes after H adsorption. Considering the Pd–Pd COOP curves (Fig. 4e–f, 5a and 6e–f) some bonding states between E_F and −5 eV disappear or decrease. This can also be noted for Pd_1–Ga_2 on the (100) surface. The Pd–Pd and Pd–Ga bonds distances are increased about 2%. The Pd–H COOP curves in Fig. 5g and h indicate a bonding interaction at −6.0 eV for both Pd_i and Pd_{ii}, which is consistent with the fact that H is bonded to two Pd atoms. In the case of the (100) surface, two peaks at −4.5 and −8.8 eV (see Fig. 4h) indicate the Pd_1–H_1 bonding interaction. There is also some Ga–H bonding interaction at −8.8 eV. Finally, a bonding peak at −6.2 eV is detected for Pd_I–H_I in the $(\bar{1}\bar{1}\bar{1})$ surface (see Fig. 6h) and at −5 eV for the subsurface H on a Pd trimmer (see Fig. 7h).

Finally, we also computed the vibration frequency of surface-bonded H. We used a whole vibrational mode with a contribution for Pd–H. The results are presented in Table 3. Vibrations frequency values are closer in (100) and (111) surfaces (1289.9 and 1206.2 cm^{-1} respectively), when compared to top adsorption on the $(\bar{1}\bar{1}\bar{1})$ surface (1786.1 cm^{-1}). This last frequency is similar to the one reported for another on-top adsorption in the PdGa(110) plane (1669.8 cm^{-1}) [4]. This last result also present some analogy with those reported by Tómanek et al. for H/Pd(100) [42]. The Pd–H vibration frequencies computed by this authors are 621, 1355 and 1750 cm^{-1} for the hollow, bridge and top sites respectively [48]. Similar values were also computed by Lovkin & Olsen for H/Pd(111) [49]. Andrews et al. reported a computed vibration frequencies of 1750.54 cm^{-1} and 1269.5 cm^{-1} for H bonded in a bridge geometry with a Pd–H–Pd bond angle of 108.2° and a Pd–H bond distance of 1.674 Å [41], which is close to our computed distance and bond angle in the $(\bar{1}\bar{1}\bar{1})$ surface (1.616 Å, 106.5^0). The lowest computed vibration frequency corresponds to H/Pd trimmer $(\bar{1}\bar{1}\bar{1})$ subsurface hollow site with a value of 633.5 cm^{-1}. Unfortunately, and to the best our knowledge, there are no experimental infrared adsorption data available to compare our computed results.

4. Conclusion

The adsorption of H in $P2_13$ PdGa intermetallic surfaces was studied by DFT calculations. The adsorption of H on (100), (111) and $(\bar{1}\bar{1}\bar{1})$ is more favorable on Pd sites at different geometries. A tilt angle is computed in the case of the (100) and (111) surfaces while $(\bar{1}\bar{1}\bar{1})$ presents an atop geometry on a Pd atom and a subsurface H interaction on a Pd trimmer, as previously reported in the literature. A Ga–H top interaction is only detected on the (100) surface. This interaction is 0.20 eV more favorable than the less favorable Pd site (atop site on the (111) surface).

The Pd–H bond is developed at the expenses of the Pd–Pd bond. Bonding contributions involve s–s and s–p orbitals with less participation of Pd 4d orbitals. The vibration frequencies computed can be compared to molecular PdH and Pd_2H_2 species in vacuum supporting the idea of isolated Pd sites with Ga acting mainly as a spacer. However, there is some Ga–H interaction similar to the one reported for Ga_2H_2 compounds.

Acknowledgements

Our work was supported by ANPCyT through PICT 1770, and PIP-CONICET No.114-200901-00272 and No.114-200901-00068 research grants, as well as by SGCyT-UNS and CIC-BA. A. J., E. A. G., J.S.A and P. V. J. are members of CONICET. P. B. is fellow researcher at this institution.

REFERENCES

[1] Kovnir K, Armbrüster M, Teschner D, Venkov T, Jentoft F, Knop-Gericke A, et al. A new approach to well-defined, stable and site-isolated catalysts. Sci Technology Adv Mat 2007;8:420–7.
[2] Klanjöek M, Gradiöek A, Kocjan A, Bobnar M, Jeglič P, Wencka M, et al. PdGa intermetallic hydrogenation catalyst: an NMR and physical property study. J Phys Condens Matter 2012;24:85703–11.
[3] Kovnir K, Armbrüster M, Teschner D, Venkov T, Szentmiklósi L, Jentoft F, et al. In situ surface characterization of the intermetallic compound PdGa – a highly selective hydrogenation catalyst. Surf Sci 2009;603:1784–92.
[4] Bechthold P, Jasen P, González E, Juan A. Hydrogen adsorption on PdGa(110): a DFT study. J Phys Chem C 2012;116:17518–24.
[5] Figueras F, Coq B. Hydrogenation and hydrogenolysis of nitro-, nitroso-, azo-, azoxy- and other nitrogen-containing compounds on palladium. J Mol Catal A Chem 2001;173:223–30.
[6] Osswald J, Kovnir K, Armbrüster M, Giedigkeit R, Jentoft R, Wild U, et al. Palladium–gallium intermetallic compounds for the selective hydrogenation of acetylene. Part II: surface

characterization and catalytic performance. J Catal 2008;258:219–27.
[7] Osswald J, Giedigkeit R, Jentoft R, Armbrüster M, Girgsdies F, Kovnir K, et al. Palladium–gallium intermetallic compounds for the selective hydrogenation of acetylene. Part I: preparation and structural investigation under reaction conditions. J Catal 2008;258:210–8.
[8] Armbrüster M, Kovnir K, Behrens M, Teschner D, Grin Y, Schlögl R. Pd-Ga intermetallic compounds as highly selective semi-hydrogenation catalysts. J Am Chem Soc 2010;132:14745–7.
[9] Armbrüster M, Kovnir K, Grin Y, Schlögl R. Complex metallic phases in catalysis. In: Complex metallic alloys – fundamentals and applications. Hoboken: Wiley-VCH; 2011.
[10] Bechthold P, Jasen P, Ardenghi J, González E, Juan A. Ab initio study of CO adsorption on PdGa(110). Comp Mater Sci 2013;71:192–6.
[11] Armbrüster M, Behrens M, Cinquini F, Föttinger K, Grin Y, Haghofer A, et al. How to control selectivity of palladium-based catalysts in hydrogenation reactions: the role of subsurface chemistry. Chem Cat Chem 2012;4:1048–63.
[12] Koc H, Yildirim A, Deligoz E. Ab initio calculations of the elastic, electronic, optical, and vibrational properties of PdGa compound under pressure. Chin Phys B 2012;21(097102):1–8.
[13] Krajčí M, Hafner J. Structure and chemical reactivity of polar three-fold surfaces of GaPd: a density-functional study. J Chem Phys 2013;138(124703):1–20.
[14] Prinz J, Gaspari R, Pignedoli CA, Vogt J, Gille P, Armbrüster M, Brune H, Gröning O, Passerone D, Widmer R. Isolated Pd sites on the intermetallic PdGa(111) and PdGa $(\bar{1}\bar{1}\bar{1})$ model catalyst surfaces. Angew Chem Int Ed 2012;51:1–6.
[15] Rosenthal D, Widmer R, Wagner R, Gille P, Armbrüster M, Grin Y, Schlögl R, Gröning O. Surface investigation of intermetallic PdGa $(\bar{1}\bar{1}\bar{1})$. Langmuir 2012;28:6848–56.
[16] Armbrüster M, Borrmann H, wedel M, Prots Y, Giedigkeit R, Gille P. Z Kristallogr NCS 2010;225:617–8.
[17] Krajčí M, Hafner J. The (210) surface of intermetallic B20 compound GaPd as a selective hydrogenation catalyst: a DFT study. J Catal 2012;295:70–80.
[18] Verbeek BH, Larsen PK, Gerits MW. Electronic structure of PdGa(110) by photoemission spectroscopy. Vacuum 1983;33:813–4.
[19] Ghasemzadeh K, Liguori S, Morrone P, Iulianelli A, Piemonte V, Babaluo A A, Basile A. H2 production by low pressure methanol steam reforming in a dense Pd–Ag membrane reactor in co-current flow configuration: experimental and modeling analysis. http://dx.doi.org/10.1016/j.ijhydene.2013.06.001.
[20] Iulianelli A, Longo T, Basile A. Methanol steam reforming reaction in a Pd–Ag membrane reactor for CO-free hydrogen production. Int J Hydrogen Energy 2008;33:5583–8.
[21] Basile A, Tereschenko GF, Orekhova NV, Ermilova MM, Gallucci F, Iulianelli A. An experimental investigation on methanol steam reforming with oxygen addition in a flat Pd–Ag membrane reactor. Int J Hydrogen Energy 2006;31:1615–22.
[22] Gallucci F, Basile A. Pd–Ag membrane reactor for steam reforming reactions: a comparison between different fuels. Int J Hydrogen Energy 2008;33:1671–87.
[23] Bobadilla LF, Palma S, Ivanova S, Domínguez MI, Romero-Sarria F, Centeno MA, et al. Steam reforming of methanol over supported Ni and Ni–Sn nanoparticles. Int J Hydrogen Energy 2013;38:6646–56.
[24] Friedrich M, Penner S, Heggen M, Armbrüster M. High CO_2 selectivity in methanol steam reforming through ZnPd/ZnO teamwork. Angew Chem 2013;125:4485–8.
[25] Föttinger K. The effect of CO on intermetallic PdZn/ZnO and Pd_2Ga/Ga_2O_3 methanol steam reforming catalysts: a comparative study. Catal Today 2013;208:106–12.
[26] Rameshan C, Stadlmayr W, Penner S, Lorenz H, Mayr L, Hävecker M, et al. In situ XPS study of methanol reforming on PdGa near-surface intermetallic phases. J Catal 2012;290:126–37.
[27] Hellner E, Laves F. Kristallchemie des In und Ga in Legierungen mit einigen Übergangselementen (Ni, Pd, Pt, Cu, Ag und Au). Z Naturforsch A 1947;2:177–83.
[28] Bhargava MK, Gadalla AA, Schubert K. Koexistente phasen vom FeSi-Typ in den mischungen Ni-Pd-Ga und Ni-Pt-Ga. J Less-Comm Met 1975;42:69–76.
[29] Phragmen G. Om jârn-kisellegeringarnas byggnad. Jernkontor Ann 1923;107:121.
[30] Kresse G, Hafner J. Ab initio molecular dynamics for liquid metals. Phys Rev B 1993;47:558–61.
[31] Kresse G, Furthmüller J. Efficient iterative schemes for *ab initio* total-energy calculations using a plane-wave basis set. Phys Rev B 1996;54:11169–86.
[32] Kresse G, Furthmüller J. Efficiency of ab-initio total energy calculations for metals and semiconductors using a plane-wave basis set. Comput Mater Sci 1996;6:15–50.
[33] Vanderbilt D. Soft self-consistent pseudopotentials in a generalized eigenvalue formalism. Phys Rev B 1990;41:7892–5.
[34] Perdew J, Chevary JA, Vosko SH, Jackson KA, Pederson MR, Singh DJ, et al. Atoms, molecules, solids, and surfaces: applications of the generalized gradient approximation for exchange and correlation. Phys Rev B 1992;46:6671–87.
[35] Monkhorst HJ, Pack JD. Special points for Brillouin-zone integrations. Phys Rev B 1976;13:5188–92.
[36] Bader RFW. Atoms in molecules: a quantum theory. Oxford: Oxford University Press; 1990.
[37] Huber KP, Hertzberg G. Molecular spectra and molecular structure IV: constants of diatomic molecules. New York: Van Norstrand Reinhold; 1979.
[38] Hoffmann R. Solid & surface: a chemist's view of bonding in extended structures. New York: Wiley-VCH; 1989.
[39] Ordejón P, Artacho E, Soler JM. Self-consistent order-*N* density-functional calculations for very large systems. Phys Rev B 1996;53:R10441–4.
[40] Soler JM, Artacho E, Gale JD, Garcia A, Junquera J, Ordejón P, et al. The SIESTA method for ab initio order-N materials simulation. J Phys Cond Matter 2002;14:2745–79.
[41] Andrews L, Wang X, Alikhani ME, Manceron L. Observed and Calculated infrared spectra of $Pd(H_2)_{1,2,3}$ complexes and palladium hydrides in solid Argon and Neon. J Phys Chem A 2001;105:3052–63.
[42] Tománek D, Sun Z, Louie SG. Ab initio calculation of chemisorption systems: H on Pd(001) and Pd(110). Phys Rev B 1991;43:4699–713.
[43] Ledentu V, Dong W, Sautet P, Kresse G, Hafner J. H-induced reconstructions on Pd(110). Phys Rev B 1998;57:12482–91.
[44] Dong W, Ledentu V, Saute P, Kresse G, Hafner J. A theoretical study of the H-induced reconstructions of the Pd(110) surface. Surf Sci 1997;377–379:46–61.
[45] Ahmed F, Alam K, Miura R, Suzuki A, Tsuboi H, Hatakeyama N, et al. Modeling of hydrogen vacancy for dissociative adsorption of H_2 on Pd (111) surface by a quantum chemical molecular dynamics. Catal Today 2011;164:16–22.
[46] Gladys MJ, Kambali I, Karolewski MA, Soon A, Stampfl C, O'Connor1 DJ. Comparison of hydrogen and deuterium adsorption on Pd(100). J Chem Phys 2010;132(024714):1–8.
[47] Himmel H-J, Manceron L, Downs AJ, Pullumbi P. Formation and characterization of the gallium and indium subhydride

molecules Ga_2H_2 and In_2H_2: a matrix isolation study. J Am Chem Soc 2002;124:4448–57.

[48] Tomanek D, Luie SG. Ab initio calculation of coverage-dependent adsorption properties of H on Pd(001). Phys Rev Lett 1986;57:2594–7.

[49] LØvik OM, Olsen RA. Adsorption energies and ordered structures of hydrogen on Pd(111) from density-functional periodic calculations. Phys Rev B 1998;58:10890–1898.